This article has been accepted for inclusion in a future issue of this journal. Content is final as presented, with the exception of pagination.

Analyzing the Power Collection Efficiency of Solar Cells by Voltage-Dependent Luminescence Imaging

Ernest I. Obetta, Jonathan Werner, Andreas Gerber, Vladimir Smirnov, Uwe Rau, and Bart E. Pieters

***Abstract*—In this study, we present a power-centric enhancement to current collection efficiency (CCE) mapping, introducing the concept of *power collection efficiency* (PCE). CCE, defined as the derivative of the cell current with respect to locally generated current, quantifies current transport efficiency (ranging from 0 to 1) to the device terminals. Traditionally, current efficiency maps are generated via electroluminescence imaging. Here, we propose generating PCE maps that quantify the ratio of locally generated power within the solar cell to the extracted power at the contacts. This approach captures both current and voltage losses, providing a more comprehensive assessment of power dissipation mechanisms. We demonstrate the proposed method on a silicon heterojunction solar cell under constant illumination, highlighting its potential for detailed, spatially resolved power loss diagnostics.**

***Index Terms*—Current collection efficiency (CCE), electro-modulated photoluminescence (EM-PL), electroluminescence (EL), power collection efficiency (PCE), power losses.**

I. Introduction

In RECENT years, electroluminescence (EL) and photoluminescence (PL) imaging have remained essential tools for solar cell characterization [1], [2]. The efficiency of photovoltaic devices is significantly influenced by the capacity to collect photo-generated carriers across the active area without substantial recombination or transport losses. Current collection efficiency (CCE) mapping has emerged as a valuable characterization technique [3], [4], [5] that provides spatially resolved information on carrier collection within solar cells, material nonuniformities, structural defects, or device-related inefficiencies that limit performance.

CCE is a differential measure ranging from 0 to 1, defined as the derivative of the terminal current with respect to the locally generated current. It quantifies how effectively the current generated locally is transported to the terminal contacts, thus serving as a direct metric for current losses. Differential EL imaging, which uses EL or electro-modulated photoluminescence (EM-PL) images taken at closely spaced bias voltages, has proven to be an effective method for obtaining CCE maps [3], [4], [6].

An alternative method for mapping the CCE is light beam-induced current (LBIC) [7]. LBIC not only allows for the determination of CCE, but can also, as demonstrated by Mundt et al. [8] in perovskite solar cells, be extended to map local power conversion efficiency.

In this work, we extend the concept of CCE by introducing a new metric, termed *power collection efficiency (PCE)*. This metric is defined as the derivative of the power extracted at the contacts with respect to the locally generated power, thus accounting for both current and voltage losses. As a result, PCE provides a more comprehensive analysis of the power transport losses in solar cells. We demonstrate that PCE maps can be readily generated using an approach similar to conventional CCE mapping techniques, employing EM-PL imaging. To demonstrate this method, we apply it to a silicon heterojunction (SHJ) solar cell under constant illumination and illustrate its effectiveness in providing spatially resolved insights into power losses.

The rest of this article is organized as follows. Section II summarizes the theory of CCE as published in [4]. In Section III, we introduce our new PCE method. Section IV describes the experimental procedures performed. Section V presents and discusses the results obtained. Finally, Section VI concludes this article with a summary of the findings and their implications.

II. Theory

The theory behind CCE mapping is based on two reciprocity theorems. The first theorem, widely used for quantitative EL imaging, relates the solar cell quantum efficiency to its luminescence, as expressed in [9]

$$\phi_{\mathrm{em}}(E) = Q_e(E)\phi_{\mathrm{bb}}(E)\left[\exp\left(\frac{V_{\mathrm{j}}}{V_{\mathrm{th}}}\right) - 1\right] + \phi_{\mathrm{sc}}(E) \quad (1)$$

where $\phi_{\mathrm{em}}(E)$ is the emitted photon flux density, $Q_e(E)$ is the quantum efficiency, $\phi_{\mathrm{bb}}(E)$ is the spectral photon flux density of a black body, V_{j} is the junction voltage, V_{th} is the thermal voltage, and $\phi_{\mathrm{sc}}(E)$ is the luminescence at short-circuit conditions.

At sufficiently large junction voltages, the expression in (1) is dominated by the exponential term, allowing the emitted photon flux to be approximated as

$$\phi_{\mathrm{em}}(E) \approx Q_e(E)\phi_{\mathrm{bb}}(E)\exp\left(\frac{V_{\mathrm{j}}}{V_{\mathrm{th}}}\right). \quad (2)$$

Received 31 May 2025; revised 26 August 2025; accepted 11 September 2025. This work was supported by the German Federal Ministry of Education and Research (BMBF) through the HGF LLEC project and the YESPVNigBen project under Grant 03SF0576A. *(Corresponding author: Bart E. Pieters.)*

Ernest I. Obetta and Uwe Rau are with the Institute of Energy Materials, Devices (IMD3-Photovoltaics), Forschungszentrum Jülich, 52425 Jülich, Germany, and also with the Jülich Aachen Research Alliance (JARA-Energy), Faculty of Electrical Engineering, Information Technology, RWTH Aachen University, 52062 Aachen, Germany.

Jonathan Werner, Andreas Gerber, Vladimir Smirnov, and Bart E. Pieters are with the Institute of Energy Materials, Devices (IMD3-Photovoltaics), Forschungszentrum Jülich, 52425 Jülich, Germany (e-mail: b.pieters@fz-juelich.de).

Digital Object Identifier 10.1109/JPHOTOV.2026.3667882

© 2026 The Authors. This work is licensed under a Creative Commons Attribution 4.0 License. For more information, see https://creativecommons.org/licenses/by/4.0/

This article has been accepted for inclusion in a future issue of this journal. Content is final as presented, with the exception of pagination.

Based on (2), junction voltage imaging is achieved by calculating the junction voltage from the camera signal, S_{cam}

$$V_{\mathrm{j}}(\boldsymbol{r}) = V_{\mathrm{th}} \ln\left(S_{\mathrm{cam}}(\boldsymbol{r}) - S_{\mathrm{cam,bg}}(\boldsymbol{r})\right) + C \tag{3}$$

where $\boldsymbol{r}$ is the spatial location within the cell, $S_{\mathrm{cam,bg}}$ is the background image acquired at 0 V bias with the same illumination conditions and exposure time as S_{cam}, and C is a calibration constant. Under the employed exposure times and illumination, the remaining PL signal in the background image was negligible. We approximate the terminal voltage as equal to the junction voltage at open-circuit to determine the value of C. More accurate calibration techniques using a calibrated light source are described in [10] and [11].

The second reciprocity theorem, derived by Wong and Green [12] for a linearized equivalent circuit of a solar cell, defines the CCE as

$$f_{\mathrm{c}}(\boldsymbol{r}) = \left.\frac{\delta I_{\mathrm{T}}}{\delta I_{\mathrm{L}}(\boldsymbol{r})}\right|_{\delta V_{\mathrm{T}}=0} = \left.\frac{\delta V_{\mathrm{j}}(\boldsymbol{r})}{\delta V_{\mathrm{T}}}\right|_{\delta I_{\mathrm{L}}(\boldsymbol{r})=0}. \tag{4}$$

Equation (4) defines the CCE as the derivative of the terminal current I_{T} with respect to a locally generated current $I_{\mathrm{L}}(\boldsymbol{r})$, effectively measuring the efficiency with which locally generated current is collected. Furthermore, (4) reveals that this efficiency is equal to the derivative of the local junction voltage with respect to the terminal voltage V_{T}. This is particularly significant as the junction voltage can be experimentally determined through EL measurements, using (3).

Combining (3) and (4), the CCE is experimentally determined as:

$$f_{\mathrm{c}}(\boldsymbol{r}) = \ln\left(\frac{S_{\mathrm{cam},1} - S_{\mathrm{cam,bg}}}{S_{\mathrm{cam},2} - S_{\mathrm{cam,bg}}}\right)\frac{V_{\mathrm{th}}}{\delta V_{\mathrm{T}}} \tag{5}$$

where $S_{\mathrm{cam},1}$ and $S_{\mathrm{cam},2}$ are the camera signals captured at small voltage steps ($\delta V_{\mathrm{T}}/2$) above and below the operating point V_{T}, respectively, and $S_{\mathrm{cam,bg}}$ is the background image.

III. Power Collection Efficiency

In this work, we extend the concept of CCE by introducing the concept of *PCE*. The PCE is defined as

$$\begin{aligned} f_{\mathrm{p}}(\boldsymbol{r}) &= \left.\frac{V_{\mathrm{T}}}{V_{\mathrm{j}}(\boldsymbol{r})}\frac{\delta I_{\mathrm{T}}}{\delta I_{\mathrm{L}}(\boldsymbol{r})}\right|_{\delta V_{\mathrm{T}}=0} = f_{\mathrm{c}}(\boldsymbol{r})\frac{V_{\mathrm{T}}}{V_{\mathrm{j}}(\boldsymbol{r})} \\ &= f_{\mathrm{c}}(\boldsymbol{r})v(\boldsymbol{r}) \end{aligned} \tag{6}$$

where $v(\boldsymbol{r}) = V_{\mathrm{T}}/V_{\mathrm{j}}(\boldsymbol{r})$ is the *voltage efficiency*. Thus, the PCE can be expressed as the product of the CCE, $f_{\mathrm{c}}(\boldsymbol{r})$, and the voltage efficiency v. Note that for a solar cell under normal operating conditions (generating power), the voltage efficiency is between 0 and 1 as under these conditions, the junction voltage is higher than the terminal voltage. The PCE, therefore, represents the ratio between the change in collected power at the contacts, $V_{\mathrm{T}}\delta I_{\mathrm{T}}$, and the change in locally generated power, $V_{\mathrm{j}}(\boldsymbol{r})\delta I_{\mathrm{L}}(\boldsymbol{r})$. As such, the PCE serves as a measure of how effectively the locally generated power is transported to the contacts.

IV. Experimental

EM-PL measurements were conducted in a light-tight cabinet to minimize ambient light interference. An 808-nm diode laser served as the illumination source. The laser beam was expanded to approximately $20 \times 20\,\mathrm{cm}^2$ at the sample plane and homogenized to ensure uniformity. The nonuniformity of the illumination across the sample area was less than 5%. For all measurements, the laser intensity was calibrated to match the short-circuit current (I_{sc}) under standard test conditions.

To detect the luminescence signal, we utilized a 4.1-megapixel silicon backside-illuminated CMOS sensor camera from Ximea (MJ042MR-GP-P6-BSI). The sensor was cooled to $-20\,^{\circ}\mathrm{C}$ throughout all measurements in this study to reduce noise and enhance signal quality. An infrared long-pass filter with a cut-on wavelength of 850 nm was employed to block the laser light and ensure accurate luminescence detection.

Both collection efficiency methods were performed on a high-efficiency quarter M2-sized SHJ solar cell (cell area: $60.5\,\mathrm{cm}^2$) [13]. The SHJ solar cell was contacted using smart wire technology and contact ribbons, and it was encapsulated with flexible polymer foils. To mitigate temperature increases in the device under test over the duration of the measurements, the sample was stabilized at an elevated temperature of 65 °C using a temperature-controlled sample holder.

A Keithley 228 source-measure unit was employed to apply a bias voltage to the sample and measure the corresponding current. For each bias voltage, both a luminescence image and a background image were captured.

V. Results

A. Imaging of Power Collection

In Fig. 1(a)–(c), we present a sequence of captured EM-PL images at three operating points: the maximum power point ($V_{\mathrm{T,mpp}} = 560\,\mathrm{mV}$), open circuit ($V_{\mathrm{T,oc}} = 680\,\mathrm{mV}$), and above open circuit ($V_{\mathrm{T}} = 700\,\mathrm{mV}$), respectively. Correspondingly, in Fig. 1(d)–(f), we show the associated junction voltage images for each operating condition.

The EM-PL and junction voltage images indicate that this particular cell exhibits slight series resistance issues at the edges. This is observed as brighter regions in the MPP images [see Fig. 1(a) and (d)] and darker regions in the above open-circuit images [see Fig. 1(c) and (f)]. Such behavior is characteristic of series resistance effects: below open-circuit, the series resistance enhances the junction voltage, while above open-circuit, due to the change in the sign of the current, it reduces the junction voltage.

Fig. 2(a)–(c) exemplarily shows the CCE maps at MPP, open-circuit and above open-circuit, respectively. The most striking feature is the strong reduction in CCE at open-circuit and above open-circuit compared to at the maximum power point. This behavior is expected, as the enhanced recombination in the solar cell at open-circuit reduces the CCE. Another notable observation is that the regions affected by series resistance, as seen in Fig. 1, exhibit lower CCE.

This article has been accepted for inclusion in a future issue of this journal. Content is final as presented, with the exception of pagination.

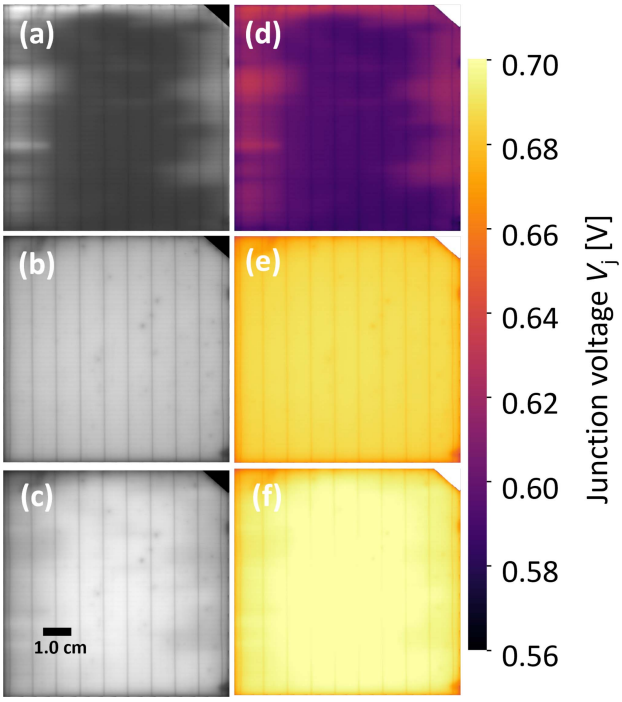


Fig. 1. Left column (a)–(c): EM-PL images of an SHJ cell at $V_{\mathrm{T,Mpp}} = 560\,\mathrm{mV}$, $V_{\mathrm{T,oc}} = 680\,\mathrm{mV}$, and $V_{\mathrm{T}} = 710\,\mathrm{mV}$. Right column (d)–(f): Calculated junction voltage images at the corresponding bias voltages.

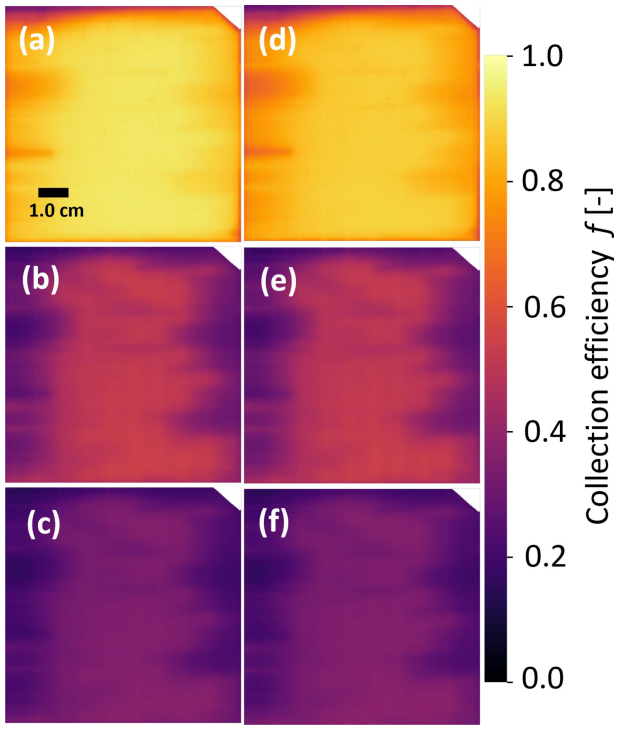


Fig. 2. Left column (a)–(c): Calculated CCE images of an SHJ cell at $V_{\mathrm{T,Mpp}} = 560\,\mathrm{mV}$, $V_{\mathrm{T,oc}} = 680\,\mathrm{mV}$, and $V_{\mathrm{T}} = 710\,\mathrm{mV}$. Right column (c)–(f): Calculated PCE images at the corresponding bias voltages.

Fig. 2(d)–(f) shows the corresponding PCE maps at MPP, open-circuit and above open-circuit, respectively. Overall, the PCE exhibits similar trends to the CCE. However, it is interesting to note that the open-circuit current and power collection efficiencies are nearly identical. This is expected because the junction voltage at open-circuit is almost uniform across the cell area and equal to the terminal voltage. Hence, the voltage efficiency v, as seen in (6), is nearly 1 across the entire cell area. Note that the voltage efficiency can exceed 1 when the terminal voltage is above the open-circuit voltage. Also, above open-circuit, the measured CCE and PCE are nearly identical. This is because the voltage is still close to open-circuit conditions.

At MPP, the PCE is slightly lower than the CCE. This discrepancy reflects the fact that at MPP, there are not only current losses (as measured by the CCE) but also voltage losses as reflected by the voltage efficiency. The PCE, being sensitive to both current and voltage losses, thus provides a more comprehensive quantification of transport losses in the solar cell.

B. Discussion

To verify the obtained collection efficiency maps, we can compare the CCE maps to the overall CCE obtained from current–voltage measurements. To this end, we use (4), which shows that we can experimentally determine the overall CCE by varying the irradiance level and forming the partial derivative of the terminal current with respect to the photocurrent. Assuming that the short circuit current equals the photocurrent

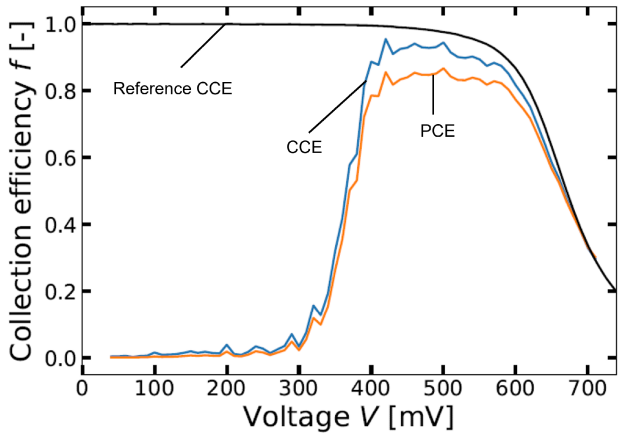


Fig. 3. Photocurrent and power collection efficiencies at various operating voltages. The black curve denotes the reference photocurrent efficiency determined through electrical measurements.

($I_{\mathrm{L}} = I_{\mathrm{T}}(0)$) at a particular irradiance level, we approximate

$$f_{\mathrm{c}} \approx \frac{I_{\mathrm{T}}(V)|_{1.0\,\mathrm{suns}} - I_{\mathrm{T}}(V)|_{0.8\,\mathrm{suns}}}{I_{\mathrm{T}}(0)|_{1.0\,\mathrm{suns}} - I_{\mathrm{T}}(0)|_{0.8\,\mathrm{suns}}}. \tag{7}$$

Fig. 3 is a plot of the photocurrent efficiency as a function of voltage (black curve). For this measurement, we varied the irradiation on the cell from a full to 80% intensity AM1.5 spectrum irradiation.

The overall CCE is compared to the CCE maps, as obtained in Fig. 2(a)–(c). To this end, we compute the mean CCE over the cell area. The resulting overall CCE is shown in Fig. 3 (blue line).

This article has been accepted for inclusion in a future issue of this journal. Content is final as presented, with the exception of pagination.

Near 700 mV, the overall CCE from CCE mapping experiments matches perfectly with the CCE from current–voltage measurements. At lower voltages, we see an increasing deviation, where down to 400 mV, the differences are relatively small. Below this voltage, the CCE from CCE mapping rapidly drops to 0.

There are two possible reasons for the discrepancies observed between the average CCE extracted from EM-PL images and the CCE obtained from electrical measurements: 1) At low voltages, the EM-PL signal is weak, resulting in a poor signal-to-noise ratio in the primary EM-PL images. Consequently, the differences between noisy images can produce unphysical results. 2) The Wong–Green network theorem [12], which underlies the present analysis, ceases to be valid at low voltages where carrier collection becomes kinetically limited. As demonstrated in [14], applying this theorem in such conditions yields apparent CCE values that approach zero and do not reflect the actual physical behavior, since (4) no longer holds in this regime.

The overall PCE is not directly obtainable from standard current–voltage experiments, as its definition includes the junction voltage [see (6)]. For completeness, we also present the PCE in Fig. 3 (orange line). As previously discussed, the PCE remains below the CCE for all voltages below open-circuit due to a voltage efficiency less than unity. Fig. 3 demonstrates that between 600 and 700 mV, the PCE and CCE are nearly identical, a finding also consistent with observations in Fig. 2. To further investigate the behavior observed in Fig. 3, we analyze histograms of CCE and PCE maps in Fig. 4. While Fig. 3 presents only the mean CCE or PCE, histograms provide a more comprehensive representation of the CCE and PCE data.

Fig. 4(a) shows the histogram of CCE and PCE at a bias voltage of $V_{\mathrm{T}} = 300\,\mathrm{mV}$. As discussed previously, the evaluation of EM-PL data at such low voltages yields unreliable results. Both histograms exhibit broad, featureless distributions, with significant portions exceeding unity or falling below zero—outcomes that are physically impossible and plausibly attributable to noise. We therefore conclude that the lower limit of validity for this evaluation method is determined by the poor signal-to-noise ratio of the primary EM-PL images, rather than by inherent limitations of the network theorem.

In contrast, the histograms of CCE and PCE at the maximum power point ($V_{\mathrm{T,Mpp}} = 560\,\mathrm{mV}$), as shown in Fig. 4(b), exhibit sharp peaks at CCE $= 0.93$ and PCE $= 0.87$. Notably, the PCE histogram is not a simple shift of the CCE histogram, indicating that PCE provides additional information regarding local power collection not available in the CCE maps. These histograms also display shoulders at CCE ≤ 0.91 and PCE ≤ 0.85, corresponding to the 50th percentile of the total histogram area. Using these values as thresholds to delineate well-performing (abovethreshold) and low-collection (below-threshold) regions, we find that 50.22% of the pixels fall into the abovethreshold region, with average efficiencies of CCE $= 0.925$ and PCE $= 0.874$. Thus, the well-performing regions have a PCE that is 0.05 higher than the over-all average value of 81.8% (see Fig. 3). This implies that the cell could have 6% (relative) more power conversion efficiency if it consisted only of the well-performing areas.

At the open-circuit voltage ($V_{\mathrm{T,oc}} = 680\,\mathrm{mV}$), as shown in Fig. 4(c), the 50th-percentile thresholds are CCE $= 0.461$ and PCE $= 0.457$, which are nearly identical. At this condition, both CCE and PCE histograms reveal substructure in the abovethreshold and belowthreshold regions, consistent with the expectation that these two quantities converge at open-circuit voltage.

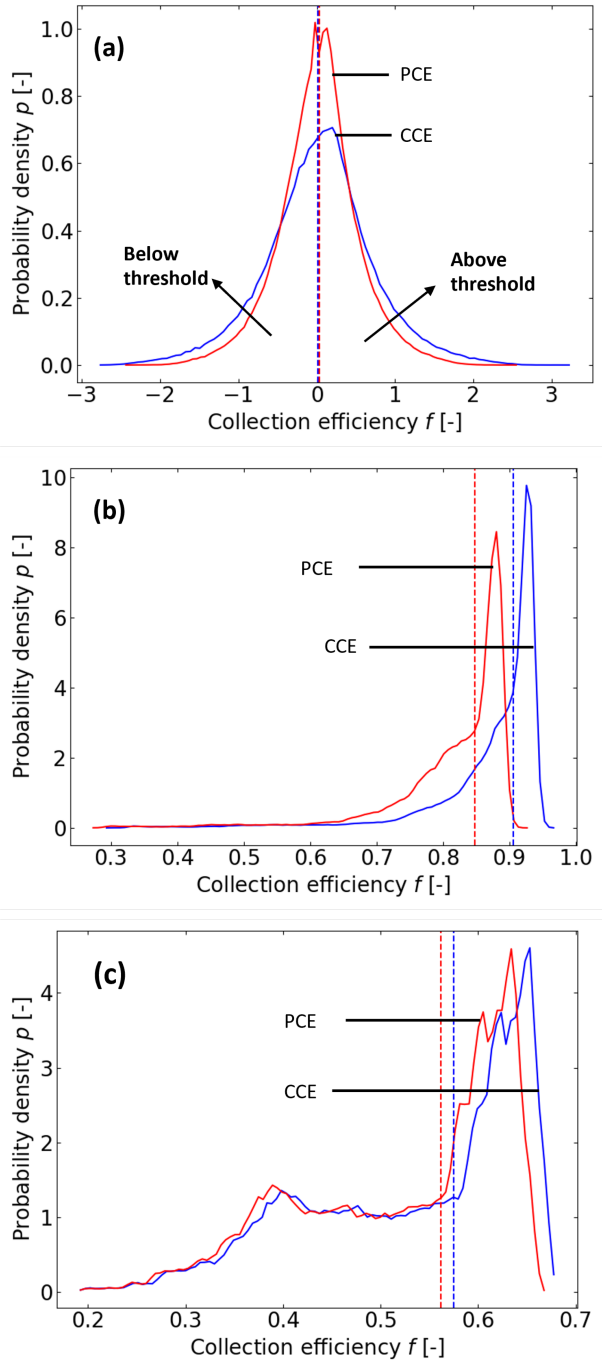


Fig. 4. Probability density histograms of collection efficiency. (a) $V_{\mathrm{T}} = 300\,\mathrm{mV}$. (b) $V_{\mathrm{T,Mpp}} = 560\,\mathrm{mV}$. (c) $V_{\mathrm{T,oc}} = 680\,\mathrm{mV}$.

VI. Summary

We introduced a new power-centric extension to the CCE method. The PCE is defined as the derivative of the ratio between the terminal current and the locally generated power. Unlike the CCE, which solely quantifies current losses, the PCE provides

This article has been accepted for inclusion in a future issue of this journal. Content is final as presented, with the exception of pagination.

a more comprehensive measure of transport losses in solar cells by equally accounting for voltage losses.

The method was demonstrated on a SHJ solar cell under constant illumination, where it was shown to provide quantitative insights into the transport power losses within the solar cell. The experiments were verified using the overall CCE obtained from current–voltage experiments. This new approach enhances our understanding of power losses and offers a valuable tool for the optimization of solar cell performance, e.g., by directly comparing the power extraction from well-performing and poorly performing areas.

ACKNOWLEDGMENT

The authors would like to thank our colleagues Andreas Lambertz and Kaining Ding for their support in supplying the SHJ samples.

REFERENCES

[1] T. Fuyuki, H. Kondo, T. Yamazaki, Y. Takahashi, and Y. Uraoka, "Photographic surveying of minority carrier diffusion length in polycrystalline silicon solar cells by electroluminescence," *Appl. Phys. Lett.*, vol. 86, Jun. 2005, Art. no. 262108.

[2] T. Trupke, R. A. Bardos, M. C. Schubert, and W. Warta, "Photoluminescence imaging of silicon wafers," *Appl. Phys. Lett.*, vol. 89, Jul. 2006, Art. no. 044107.

[3] J. Wong, R. Sridharan, Y. C. Wang, and T. Mueller, "Differential electroluminescence imaging and the current transport efficiency of silicon wafer solar cells," in *Proc. IEEE 40th Photovolt. Specialist Conf.*, 2014, pp. 0975–0979.

[4] U. Rau et al., "Photocurrent collection efficiency mapping of a silicon solar cell by a differential luminescence imaging technique," *Appl. Phys. Lett.*, vol. 105, Oct. 2014, Art. no. 163507.

[5] A. Gerber et al., "Advanced large area characterization of thin-film solar modules by electroluminescence and thermography imaging techniques," *Sol. Energy Mater. Sol. Cells*, vol. 135, pp. 35–42, 2015.

[6] V. Huhn et al., "Imaging photocurrent collection losses in solar cells," *Appl. Phys. Lett.*, vol. 109, Dec. 2016, Art. no. 223502.

[7] C. Donolato, "Theory of beam induced current characterization of grain boundaries in polycrystalline solar cells," *J. Appl. Phys.*, vol. 54, pp. 1314–1322, Mar. 1983.

[8] L. E. Mundt et al., "Quantitative local loss analysis of blade-coated perovskite solar cells," *IEEE J. Photovolt.*, vol. 9, no. 2, pp. 452–459, Mar. 2019.

[9] U. Rau, "Superposition and reciprocity in the electroluminescence and photoluminescence of solar cells," *IEEE J. Photovolt.*, vol. 2, no. 2, pp. 169–172, Apr. 2012.

[10] O. Fischer et al., "Versatile implied open-circuit voltage imaging method and its application in monolithic tandem solar cells," *Prog. Photovolt.: Res. Appl.*, vol. 33, no. 1, pp. 40–53, 2025.

[11] A. M. Soufiani et al., "Implied open-circuit voltage imaging via a single bandpass filter method—Its first application in perovskite solar cells," *Adv. Funct. Mater.*, vol. 33, no. 3, 2023, Art. no. 2210592.

[12] J. Wong and M. A. Green, "From junction to terminal: Extended reciprocity relations in solar cell operation," *Phys. Rev. B*, vol. 85, Jun. 2012, Art. no. 235205.

[13] W. Duan et al., "A route towards high-efficiency silicon heterojunction solar cells," *Prog. Photovolt.: Res. Appl.*, vol. 30, no. 4, pp. 384–392, 2022.

[14] U. Rau, V. Huhn, and B. E. Pieters, "Luminescence analysis of charge-carrier separation and internal series-resistance losses in $Cu(In, Ga)se_2$ solar cells," *Phys. Rev. Appl.*, vol. 14, Jul. 2020, Art. no. 014046.